Computational Design of Metal Surfaces and Human-Machine Collaborative Construction: Parameter-Driven Computational Design and Multi-Agent Collaborative Construction Methods for Metal Surfaces

Xiaolong Chang[1*]

[1] Guangdong Beyho Technology Co., Ltd., Foshan, 528000, China

* cxl@beyho.cn

https://doi.org/10.70695/IAAI202601A1

Abstract

The design and formation of freeform metal surfaces are disconnected, manufacturing constraints are difficult to pre-set, and human-machine collaboration efficiency is low. To address these issues, a parametrically excited computational design and multi-agent collaborative formation method for metal surfaces is developed. First, NURBS surfaces are used as the core geometric representation, and process constraints such as curvature, plate thickness, and forming radius are explicitly incorporated into the parameter space, creating a multi-objective improved model that considers geometric approximation, structural performance, and manufacturing costs. Next, a human-machine-measurement multi-agent system architecture is presented. Through task parameterization coding and collaborative scheduling strategies, the improved surface family is transformed into executable assembly tasks. Solid-state verification is conducted using six sets of templates with different curvatures and scales. The results show that when the RMSE is controlled within 4.2 mm, the total project duration is reduced by an average of approximately 22%, robot utilization is significantly improved, and the average RPE of human workers decreases by approximately 2 levels. This demonstrates that the method can ensure geometric accuracy, effectively improve manufacturing efficiency, and reduce the burden on both humans and machines.

Keywords Metallic Curved Surface; Computational Design; Multi-Agent Collaboration; Human-Machine Collaborative Construction; Geometric Accuracy

1 Introduction

In recent years, the increasing complexity of construction and manufacturing has driven the development of computational design and human-machine collaborative construction. Zheng et al. proposed a multi-agent collaborative conceptual design method for small and medium-sized manufacturing [1]. Hosmer et al. used deep multi-agent reinforcement learning to create an autonomous building ecosystem [2]. Hu et al. reviewed its decision-making advantages in engineering operation and the bottleneck of heterogeneous coordination [3]. El-Magnaby et al. focused on the value of multi-agent generative design in early morphological investigation [4]. Iannino et al. applied it to steel production to improve energy efficiency and scheduling [5]. Xiong et al. proposed a human-machine collaborative additive model [6]. Pollini and Oraskari emphasized the significance of adaptive automation in human-machine collaboration, but also indicated that the complexity of the site restricts immediacy [7-8]. Mitterberger and Dörfler advocated the digital construction of "human-machine-process" integration [9]. Kyaw et al. achieved intuitive collaboration through gestures and MR. Although intelligent collaboration, generative design and interaction methods have developed, there is still a lack of systematic methods for parameter excitation design and multi-agent creation integration of complex components such as metal curved surfaces [10]. Therefore, a parameter-centric multi-agent collaborative construction framework is constructed to achieve a closed loop of design-manufacturing-feedback. This paper proposes a parameter-excited computational design and collaborative creation method to improve the manufacturability and creation efficiency of metallic surfaces, and experimentally demonstrates the method's performance in terms of energy efficiency, accuracy, and collaborative capabilities.

2 Parametric-Driven Computational Design Method for Metallic Surfaces

2.1 Parametric Geometric Modeling of Metal Surfaces

To balance free-form representation with numerical stability, metallic surfaces are represented using a unified two-parameter NURBS/B-spline method.

$$\mathbf{S}(u,v)=\frac{\sum_{i=0}^{n}\sum_{j=0}^{m}N_{i,p}(u)M_{j,q}(v)w_{ij}\mathbf{P}_{ij}}{\sum_{i=0}^{n}\sum_{j=0}^{m}N_{i,p}(u)M_{j,q}(v)w_{ij}},\quad (u,v)\in[0,1]^2 \tag{1}$$

Where $\mathbf{S}(u,v)$ is the spatial coordinate vector of the parameter points on the surface; $N_{i,p}(u)$ and $M_{j,q}(v)$ are the B-spline basis functions of the u, v order in the directions , respectively; p, q $\mathbf{P}_{ij}$ is the coordinate of the control point; w_{ij} is the corresponding weight; and is the value of the control point after subtracting n, m one from the number of control points in the two directions. This expression is beneficial for directly obtaining geometric features such as principal curvature and surface element size.

High-level design variables are presented as parameter vectors :

$$\mathbf{p}=\left[L_x,L_y,H,\alpha_1,\ldots,\alpha_k\right] \tag{2}$$

The underlying geometric variable vectors $\mathbf{x}=f\left(\mathbf{p}\right)$ are associated through a mapping function :

$$\mathbf{x}=\left[\mathbf{P}_{00},\ldots,\mathbf{P}_{nm},w_{00},\ldots,w_{nm}\right] \tag{3}$$

Here L_x,L_y, represents the span and depth, H represents the undulation height, and α_i represents the critical polyline or boundary control angle. The mapping function automatically updates the node vectors and control network within the computational kernel. The parameter calculation process is shown in Figure 1:

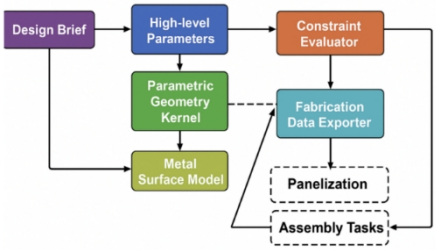

Fig. 1. Flowchart of parameter-driven computational design

2.2 Modeling of Manufacturing Constraints and Parametric Feasibility Region

Forming limits are explicitly modeled through the relationship between curvature, sheet thickness, and material strength. Typical manufacturing constraints are written as...

$$|\kappa(u,v)|\le\kappa_{\max}(\cdot)\left(t,\sigma_y\right)=\frac{1}{R_{\min}\left(t,\sigma_y\right)},\quad (u,v)\in[0,1]^2 \tag{4}$$

Where $\kappa(u,v)$ represents (u,v) the absolute value of the principal curvature of the surface at the parameter point; $\kappa_{\max}(\cdot)$ is t the maximum curvature allowed under the conditions of plate thickness $R_{\min}\left(t,\sigma_y\right)$ and material yield strength; σ_y and corresponds to the minimum bending radius. Table 1 lists the plate thickness, steel grade, upper and lower limits of curvature, bending angle range, and allowable residual strain of typical components according to surface region ID. $\varepsilon_{res,max}$ This table can be directly used for feasibility pre-screening in the parameter solution process and supports the adoption of differentiated manufacturing strategies for different regions.

Table 1. Parameters and constraint ranges of representative metallic curved surface regions

Region ID	Thickness t /mm	Steel grade	κ_{min} (1/m)	κ_{max} (1/m)	Bending angle range/°	$\varepsilon_{res,max}$ /%
R1	4.0	S235	0.00	0.40	0–60	0.25
R2	6.0	S355	0.00	0.65	0–75	0.30
R3	8.0	S355	0.00	0.85	0–90	0.35
R4	10.0	S460	0.00	1.05	0–95	0.40

2.3 Construction of Multi-Objective Optimization Design Problem

Within the feasible region , the design of metal surfaces is formulated as a multi-objective optimization problem: Ω_{feas}

$$\min_{\mathbf{p}\in\Omega_{\text{feas}}} J(\mathbf{p}) = w_1 J_{\text{geom}}(\mathbf{p}) + w_2 J_{\text{struct}}(\mathbf{p}) + w_3 J_{\text{fab}}(\mathbf{p}) \tag{5}$$

Wherein, $J_{\text{geom}}(\mathbf{p})$ is the geometric approximation error function between the target shape and the parametric surface; $J_{\text{struct}}(\mathbf{p})$ is the structural performance penalty function obtained based on finite element analysis (including displacement, stress exceeding limits, etc.); $J_{\text{fab}}(\mathbf{p})$ is the manufacturing and assembly cost function (involving the number of components, number of bends, weld length, construction time, etc.); w_1, w_2, w_3 and is a non-negative weight coefficient, which, after normalization, reflects the project's emphasis. Constraints are uniformly written as :

$$\mathbf{g}(\mathbf{p}) \le \mathbf{0}, \quad \mathbf{h}(\mathbf{p}) = \mathbf{0} \tag{6}$$

Among them, $\mathbf{g}(\mathbf{p})$ is the inequality constraint vector, which includes manufacturing constraints, surface element size constraints, and component stability conditions derived from equation (4); $\mathbf{h}(\mathbf{p})$ is the equality constraint vector, which is used to ensure that the key control points are on the specified boundaries, support lines , or symmetry planes. During the solution process, a non-dominated solution set is created using a Pareto-based multi-objective genetic algorithm, and a gradient-based local search is added later to improve convergence accuracy and the uniformity of the solution set, thereby providing stable parameter samples for subsequent surface family generation.

2.4 Surface Family Generation and Geometric Feature Analysis

In the candidate solution set obtained by multi-objective improvement, Latin hypercube sampling and clustering are used to resample the parameter vectors, thereby creating a family of surfaces containing different compromise schemes. Each parameter vector is transformed into a specific geometric model according to the rules of formulas (1) to (2), and then the principal curvature, mean curvature, Gaussian curvature and surface element size are calculated to take into account the difficulty of forming and the complexity of the structure.

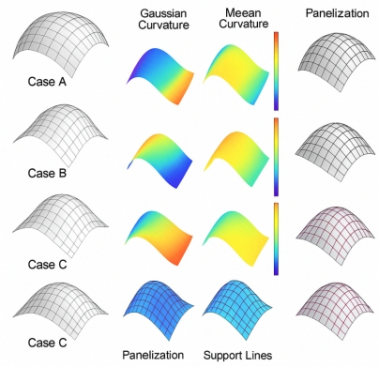

Fig. 2. Three-view diagrams of several representative curved surface examples + curvature heatmap/surface element partitioning diagram

Referring to Figure 2, cross-case comparisons clearly show that changes in parameters affect curvature concentration areas, plate size distribution, and support requirements. This provides prior geometric knowledge for component decomposition and task allocation during subsequent multi-entity collaborative creation.

3 Parameter-Driven Multi-Agent Human-Machine Collaborative Construction Method

3.1 Human-Machine-Measurement Multi-Agent System Architecture

As shown in Figure 3, based on the parametric surfaces and element partitioning mentioned earlier, the multi-agent collaborative creation system adopts a layered architecture design. The upper layer is the "Coordination and Digital Twin Layer", which receives data such as "panel data", "assembly tasks", and "tolerance diagrams" from the parametric model and improvement module, and safeguards the state of the metal surfaces and components in the virtual environment. The middle layer is called the "Execution Layer", which includes a mobile platform, a six-degree-of-freedom robotic arm , and a human operation unit; while the lower layer is named the "Perception Layer", which is formed by a laser scanner, a total station, and visual nodes, providing the upper layer with real-time geometric and state feedback information. To quantify the capabilities of each agent and their limitations, Table 2 lists the main performance parameters of multiple robots and measuring equipment, which become the input content for the task allocation and scheduling algorithm.

Table 2. Key performance data of robot and measurement system

Agent ID	Type	Workspace (m)	Payload (kg)	Positioning Accuracy (mm)	Sensing Range (m)	Sampling Rate (Hz)	Communication Period (ms)
R1	Mobile Manipulator	3.0×3.0×2.5	10	1.0	–	250	20
R2	Fixed Manipulator	2.0×2.0×1.8	15	0.5	–	500	10
S1	Laser Scanner	–	–	2.0	30	20	50
S2	Total Station	–	–	1.0	80	5	

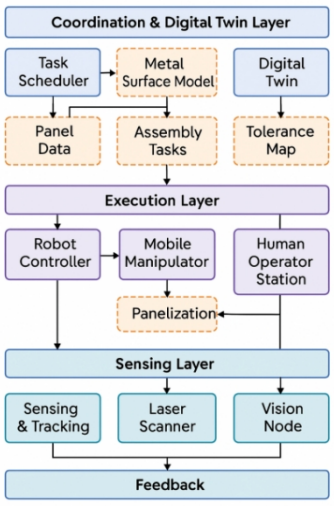

Fig. 3. Architecture diagram of a multi-entity collaborative construction system

3.2 Task Decomposition and Parameterized Task Coding

In the system architecture, the conversion of parametric surfaces and panel partitioning results into an executable assembly task set first relies on panels and support lines to automatically generate a component list and assembly topology, clarifying the target pose, installation sequence, and acceptable

assembly tolerance of each component. Next, the " Panelization " and "Support Lines" data in Figure 2 are mapped into the task graph, thus creating an assembly network with sequential and spatial constraints.

For each task k, define a task vector $\boldsymbol{\tau}_k = [ID_k, \mathbf{T}_k, \delta_k, p_k, r_k, \ldots]$ and construct a task cost function.

$$C_k = \lambda_L L_k + \lambda_T T_k + \lambda_I I_k + \lambda_R R_k \tag{7}$$

Wherein, C_k represents the comprehensive cost of task k, L_k represents the length of the movement path of the executing entity from the previous workstation to the current component installation position, T_k is the estimate of its operation time, I_k reflects the number of human-computer interactions or the complexity of the interaction, R_k is the risk or danger coefficient, takes into account factors such as high-altitude operations and the possibility of collision, λ_L , λ_T , λ_I , λ_R are the corresponding weight coefficients, after normalization, it can be ensured that they have the same dimension. After quantifying all candidate tasks according to equation (7), the cost of different allocation schemes can be directly compared in the subsequent scheduling arrangement. Combined with the equipment capabilities in Table 2, a task coding system suitable for multi-entity heterogeneous characteristics can be created.

3.3 Multi-Agent Collaboration Strategy and Online Adjustment

The multi-agent scheduling problem based on the task cost model is formulated as a constrained cooperative optimization scheduling layer that divides the task set into several batches according to the task graph and its priorities, and allocates these tasks to different robots and human units through auction-style allocation or mixed-integer programming. The relationship between the allocation scheme and task-agent matching variables, as well as the process of checking the overall cost and constraints, are discussed.

The overall collaborative goal can be written as

$$\min_{\mathbf{\Pi}} J_{coll} = \sum_k C_k(\pi_k) + \mu_W W_{idle} + \mu_H H_{load} \tag{8}$$

Where, $\mathbf{\Pi} = \{\pi_k\}$ is the set of task assignment schemes, π_k representing the undertaker of task k; $C_k(\pi_k)$ is π_k the task cost during main execution, given by equation (7); W_{idle} is the measure of total system idle time or waiting time; H_{load} is the indicator of human workload, which can be obtained by adding attitude evaluation to the cumulative working time; μ_W and μ_H are the corresponding weights. During the online phase, the measurement/scanning system will continuously update the pose of components and assembly deviations. The scheduling layer will reconsider and reconsider the constraints based on these new situations , C_k and carry out local reassignment for tasks that have not yet started or are in progress, thereby shortening the overall project duration and improving collaborative efficiency while maintaining the upper limit of human and machine workload.

4 Experimental Platform Setup, Results and Data Analysis

4.1 Experimental Platform and Test Conditions

As shown in Figure 4, the experimental platform selected six representative schemes from the aforementioned family of parametric surfaces, processed them into metal plates through CNC cutting and bending, and built physical prototypes on an adjustable steel frame. Each scenario includes a complete support system and measurement targets, with boundary conditions covering combinations of simply supported, four-sided fixed, and locally hinged joints to simulate three typical working conditions: roof, curtain wall, and shell. The human-machine collaborative construction follows the process of "robot coarse positioning+manual fine adjustment+total station/scanning verification", no longer using block diagrams, but emphasizing the actual construction path: the mobile platform first completes the plate transportation, then performs attitude pre-alignment, then the robotic arm performs temporary fixation, and the operator performs locking and fine adjustment at local nodes. Finally, the measurement system initiates the next task.

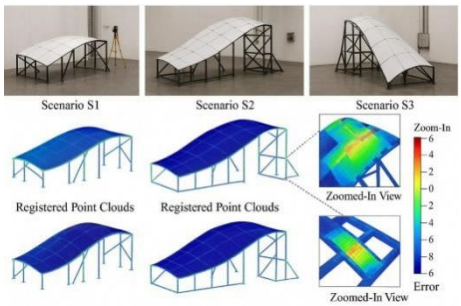

Fig. 4. Experimental platform and registration point cloud results for metal curved surface scenes S1–S3

Table 3 summarizes the test scenarios and surface parameters, including indicators such as span, camber height, maximum Gaussian curvature, composite plate thickness, number of panels, and number of support points. These will be used as reference standards for subsequent evaluation of geometric accuracy and efficiency.

Table 3. Test scenarios and surface parameter configuration

Scenario ID	Span (m)	Rise (m)	Max Gaussian Curvature (1/m²)	Plate Thickness (mm)	No. of Panels	No. of Supports
S1	8.0	1.2	0.20	4/6	42	10
S2	10.0	1.5	0.35	4/8	56	12
S3	12.0	2.0	0.50	6/8	64	14
S4	14.0	2.5	0.60	6/10	78	16
S5	16.0	3.0	0.75	8/10	92	18
S6	18.0	3.5	0.90	8/12	108	20

4.2 Geometric Accuracy and Deformation Analysis

After assembly in each scenario, a total station and laser scanning are used to acquire point clouds of the panel surface. First, the measured point cloud is registered with the design coordinate system using control points. Then, it is projected onto the target curved surface according to a unified grid to obtain the normal deviation, which is used to evaluate the installation accuracy. After the temporary supports are removed or unloaded, a second scan is performed. By using the difference between the two point clouds, the springback and residual deflection of the component can be obtained. The entire process is automatically cleaned by the "Deviation Analysis" module, outliers are removed and statistical indicators are calculated to ensure that the same evaluation criteria are used for comparison in different scenarios. Figure 5 shows the error distribution of S1-S6 on the left and the springback trend under different thickness and curvature ranges on the right. Table 4 puts the geometric error and deformation index in a data table, which gives accuracy indicators such as RMSE and maximum deviation, and also lists the average springback rate and maximum residual deflection for the corresponding scenario. This allows for observation of the coupling relationship between parameter design, forming difficulties and installation quality from the same perspective.

Table 4. Combined geometric accuracy and deformation statistics

Scenario ID	RMSE (mm)	Max Error (mm)	95th Percentile (mm)	Mean Springback (%)	Max Residual Deflection (mm)
S1	2.1	4.5	3.9	1.8	3.2
S2	2.6	4.9	4.3	2.2	3.8
S3	3.0	5.3	4.7	2.7	4.6
S4	3.4	5.8	5.1	3.3	5.4
S5	3.8	6.1	5.5	3.9	6.2
S6	4.2	6.4	5.9	4.5	7.1

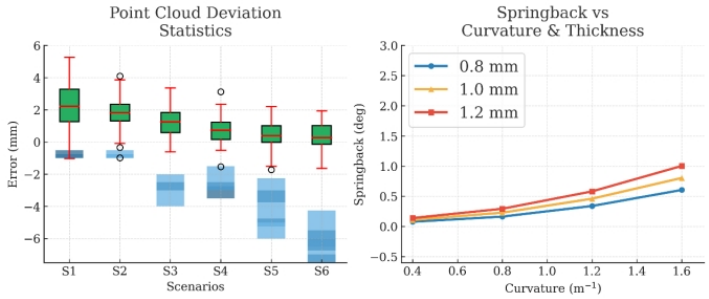

Fig. 5. Point cloud deviation statistics and relationship between springback-curvature/thickness

4.3 Assessment of Collaborative Efficiency and Human-Machine Load

Assuming the geometric accuracy requirements are met, two construction strategies are further compared: Scheme A is a "traditional manual and single-robot assisted handheld" mode, while Scheme B is a "parameter-triggered multi-agent collaborative" mode. In scenarios S1-S3, both schemes were used multiple times. The scheduling system logs recorded the task start and end times, robot operation status, and human waiting times. Furthermore, wearable heart rate monitors and video-based posture recognition were used to calculate the number of movements and the proportion of poor postures. After construction, subjective workload evaluation scores were collected . Multi-source data were aligned with the timeline in the "Performance & Workload Monitor" module to construct unified task-level metrics .

Figure 6 illustrates the differences between the two schemes in terms of comprehensive indicators (CI), total project duration, robot utilization, and average RPE, visually emphasizing the overall trade-off between efficiency and human-machine workload in multi-agent collaboration. Table 5 integrates efficiency and workload indicators into the same data table, using "scheme-scenario" combinations as rows, listing data such as total project duration, robot utilization, average heart rate improvement, number of actions, and RPE score. This table highlights the overall impact of the collaboration strategy on construction organization: while maintaining or improving geometric accuracy, the project duration is significantly shortened, the robot is more fully utilized, and both human physical labor and subjective workload decrease.

Table 5. Integrated productivity and human workload metrics

Strategy	Scenario	Total Duration (min)	Robot Utilization (%)	Avg. HR Increase (%)	Motion Count per Task	RPE Score (1–10)
A	S1	295	46	19	135	7.8
A	S2	338	43	18	131	7.5
A	S3	372	41	17	128	7.2
B	S1	228	71	11	102	5.9
B	S2	254	69	12	105	6.1
B	S3	281	67	10	97	5.6

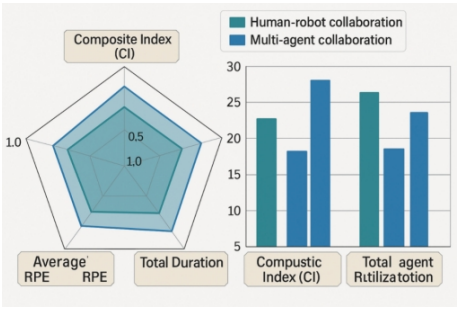

Fig. 6. Comparison of different construction strategies in terms of comprehensive indicators, total project duration, robot utilization rate, and average RPE

5 Conclusions and Outlook

Research shows that the parametrically excited computational design framework for metal surfaces can unify geometric representation, manufacturing constraints, and multi-objective improvements into a mapping relationship. This allows for clear control of key variables such as curvature, plate thickness, and forming radius within the parameter space, directly transforming the improved results into panel partitioning and support configuration schemes. Based on this design outcome, a human-machine-measurement multi-master system is formed, achieving a cyclical correlation between the design model, robot execution, and on-site measurement data through parametric coding and collaborative scheduling of tasks. The experimental platform was compared across multiple scenarios. When manufacturing constraints were met, the prototype RMSE was controlled within 4.2 mm, the total project duration was reduced by approximately 20%-25% compared to the traditional method, robot utilization was significantly improved, and both human heart rate and subjective RPE were noticeably reduced. This confirms the comprehensive advantages of the proposed method in terms of geometric accuracy, construction efficiency, and human-machine workload. The current sample size is small, and the structural types are limited. Therefore, even with the achievements, further promotion and calibration work is needed in a wider range of engineering projects using more materials, thus laying a foundation for intelligent creation of complex shell systems in the future.

Acknowledgement

This work was supported without any funding.

Conflicts of Interest

The authors declare no conflicts of interest.

References

1. Zheng, C., Du, Y., Sun, T., et al. (2023). Multi-agent collaborative conceptual design method for robotic manufacturing systems in small-and mid-sized enterprises. Computers & Industrial Engineering, 183, 109541.
2. Hosmer, T., Mutis, S., Gheorghiu, O., et al. (2024). Autonomous ecologies of construction: Collaborative modular robotic material eco-systems with deep multi-agent reinforcement learning. International Journal of Architectural Computing, 22(4), 661-688.
3. Hu, Y., Wu, L., Li, N., et al. (2024). Multi-Agent Decision-Making in Construction Engineering and Management: A Systematic Review. Sustainability, 16(16), 7132.
4. El-Maghraby, I. M., Jahin, H., Al-Hagla, K. S. M. (2023). Computational-based Generative Design Exploration, Multi-Agent System as an Approach. In LET IT GROW, LET US PLAN, LET IT GROW. Nature-based Solutions for Sustainable Resilient Smart Green and Blue Cities. Proceedings of REAL CORP 2023, 28th International Conference on Urban Development, Regional Planning and Information Society (pp. 145-154). CORP-Competence Center of Urban and Regional Planning.
5. Iannino, V., Colla, V., Mocci, C., et al. (2021). Multi-agent systems to improve efficiency in steelworks. Matériaux & Techniques, 109(5-6), 502.
6. Xiong, Y., Tang, Y., Kim, S., et al. (2023). Human-machine collaborative additive manufacturing. Journal of Manufacturing Systems, 66, 82-91.
7. Pollini, A., Giacobone, G. A., Zanoni, M., et al. (2025). Human-machine interaction design in adaptive automation. Procedia Computer Science, 253, 1034-1044.
8. Oraskari, J. T., Kirner, L., Zocklein, M., et al. (2024). Toward human-machine collaboration in autonomous material handling on construction sites. Human-Machine Communication, 9, 189-213.
9. Mitterberger, D., & Dörfler, K. (2024). Rethinking Digital Construction: A Collaborative Future of Humans, Machines and Craft. Architectural Design, 94(5), 108-117.
10. Kyaw, A. H., Spencer, L., Lok, L. (2024). Human-machine collaboration using gesture recognition in mixed reality and robotic fabrication. Architectural Intelligence, 3(1), 11.

Biographies

1. **Xiaolong Chang** Master, currently works at Guangdong Beyho Technology Co., Ltd. His main research directions include artificial intelligence robots and construction robots.

金屬曲面的計算性設計與人機協同建造參數驅動下金屬曲面的計算性設計與多主體協同建造方法

常小龍[1]

[1]廣東畢要科技有限公司，佛山，中國，528000

摘要：金屬自由曲面設計與形成存在脫節現象，製造約束難以预先設定，人機協同效率較低，針對這些情況，形成了一種參數激發的金屬曲面計算性設計與多主體協同形成一體化方法。首先把 NURBS 曲面當作核心幾何表現形式，把曲率、板厚、成形半徑這些工藝限制明確地納入到參數空間當中，創建起既考慮幾何逼近，又顧及結構性能，還牽涉製造成本的多目標改良模型。接著給出了人–機–測量多主體系統架構，經由任務參數化編碼以及協同調度策略，把改良後的曲面家族轉變成可執行裝配任務。以六組具有不同曲率和尺度的樣板展開實體驗證，結果表明當 RMSE 控制在 4.2mm 以內時，總工期平均縮減約 22%，機器人利用率明顯改進，人工平均 RPE 下降約 2 級，這顯示該方法既能保障幾何精度，又能有效地提升營造效率並且減小人機負擔。

關鍵詞：金屬曲面；計算性設計；多主體協同；人機協同建造；幾何精度

1. 常小龍，項目管理碩士，任職於廣東畢要科技有限公司，主要研究方向為人工智慧機器人、建築機器人等。